3D modeling of filtration process via polyurethane nanofiber based nonwoven filters prepared by electrospinning process

Wannes Sambaer[3], Martin Zatloukal[a]* Dusan Kimmer[b]

A B S T R A C T

Full 3D particle filtration modeling at low pressures considering slip/transition/free molecular flow regime, particle-fiber interactions, air/particle slip, sieve and homogenous flow field has been performed for the polyurethane nanofiber filter prepared by electrospinning process and the obtained theoretical predictions for the filtration efficiency have been compared with the corresponding experimental data. Moreover, the effect of air velocity, viscosity, temperature, pressure and particle-fiber friction coefficient on the produced polyurethane nanofiber filter efficiency has been investigated in more details. In order to take all real structure features of the nanofiber filter into account (such as varying fiber diameter, curvature along its length, inhomogeneity and mat defects), a new approach for 3D nano fiber mat model construction from corresponding SEM images has been proposed and utilized.

1. Introduction

During the past decades, significant progress has been done in the area of filtration science and technology (Andrady, 2008; Hosseini and Tafreshi, 2010a, b; Fotovati et al, 2010; Sambaer et al., 2010; Ashari and Tafreshi, 2009; Tafreshi et al, 2009; Jaganathan and Tafreshi, 2008; Jaganathan et al., 2008; Zobel et al., 2007; Wang et al., 2006a, b, 2007; Maze et al., 2007; McNenly et al., 2005; Pich, 1966; Li and Ahmadi, 1992; Ounis and Ahmadi, 1990; Ounis et al., 1991; Altmann and Ripperger, 1997; Rubin, 1977; Brown, 1993; Thomas and Yoder, 1956; Sinclair, 1970), which follows increased needs of many advanced industries dealing with electronics, medical, pharmaceutical and biology to maintain clean room manufacturing environments (Andrady, 2008; Brown, 1993). Nanofiber mats, having fiber diameter typically in order of tens and hundred nanometers, are very well suited for air filtration because low solidity and acceptable mechanical strength can be obtained. Moreover, due to nanoscale fiber diameter dimension, air slip flow occurs at the fiber surface, which lowers filtration pressure and increases efficiency of impaction, interception and diffusion due to increased contact of air and particles with the fiber surface (Andrady, 2008; Hosseini and Tafreshi, 2010a; McNenly et al., 2005; Brown, 1993). Even if the filters with nanofibers have relatively simple engineering construction, their aerosol collection efficiencies are not easily predictable because of the inability to precisely measure the detailed filter properties (Andrady, 2008). Thus, it is not surprising that filtration modeling has been recently utilized on the virtual simplified nanofiber mats in order to understand their behavior in more detail (Hosseini and Tafreshi, 2010a, b). However, utilization of virtual idealized nanofiber mats in filtration modeling considering constant diameter along the fiber, neglecting their curvature, inhomo- geneous features and possible defects may not sufficiently represent real nanofiber mats and thus, predictive capabilities of such models could be significantly reduced. In order to overcome this possible limitation, a new approach for real 3D nanofiber mat construction from their scanning electron microscopy (SEM) images is proposed here as the first step. This methodology is applied for manufactured polyurethane (PU) nanofiber nonwoven based filter prepared by the electrospinning process. In the next stage, full 3D particle filtration modeling using the 3D structure model representing real filter structure has been utilized considering slip/transition/free molecular flow regime, particle-fiber interactions, air/particle slip, sieve and homogenous flow field. The obtained theoretical predictions for the filtration efficiency have been compared with the corresponding experimental data. Finally, the effect of air velocity, viscosity, temperature, pressure and particle-fiber friction coefficient on the produced polyurethane nanofiber filter efficiency have been investigated.

2. Filter sample preparation and characterization

2.1. *Material*

A polyurethane solution in dimethylformamide (DMF) based on 4,4'methylenebis(phenylisocyanate) (MDI), poly(3-methyl-l,5- pentanediol)-alt-(adipic, isophtalic acid) (PAIM) and 1,4 butanediol

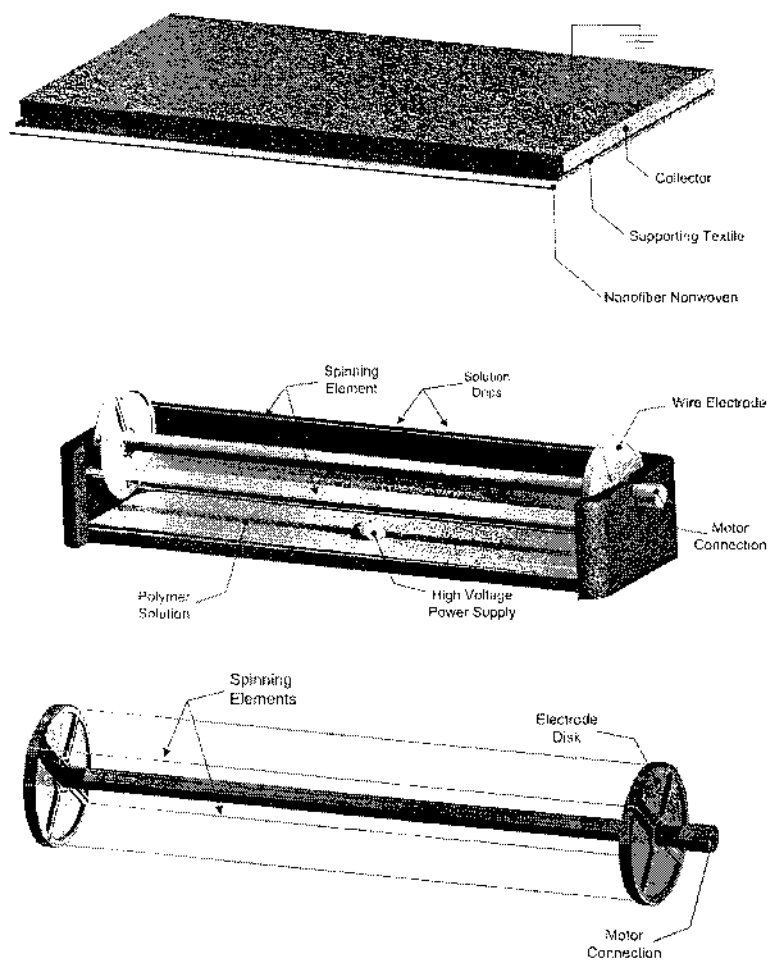

Fig. 1. Scheme of the electrospinning process (at the top) using rotating electrode with cotton cord spinning elements (at the bottom).

(BD) was synthesized in molar ratio 9:1:8 at 90 °C for 5 h (per partes way of synthesis starting with preparation of prepolymer from MDI and PAIM and followed by addition of BD, remaining quantity of MDI). The prepared solution, suitable for electrospinning process, had a PU concentration of 13.5 wt%, viscosity of 1.53 Pa s and conductivity of 146.2 (.iS/cm (adjusted by tetraethy- lammonium bromide).

2.2. *Filter sample preparation by electrospinning process*

Nanofiber nonwoven based filter sample was prepared from polyurethane solution with a commercially available NanoSpider™ machine (Elmarco s.r.o. Liberec, Czech Republic, http:// www.elmarco.com/) equipped with patented rotating electrode with 4 cotton cords spinning elements (PCT/CZ2010/000042) as shown in Fig. 1. The experimental conditions were: relative humidity 36%, temperature 22 °C, electric voltage (applied into PU solution) 75 kV, distance between electrodes 180 mm, rotational electrode speed 7 rpm and speed of supporting textile collecting nanofibers was 0.16 m/min. Nanofibers were collected on polyester fabric with square ordering of electroconductive fiber Resistat 9601, area mass 95 g/m², electroconductive thread distance was 5 mm. Samples for further analyses were taken from the middle part of the 40 cm wide fabric coated with layer of nanofibers.

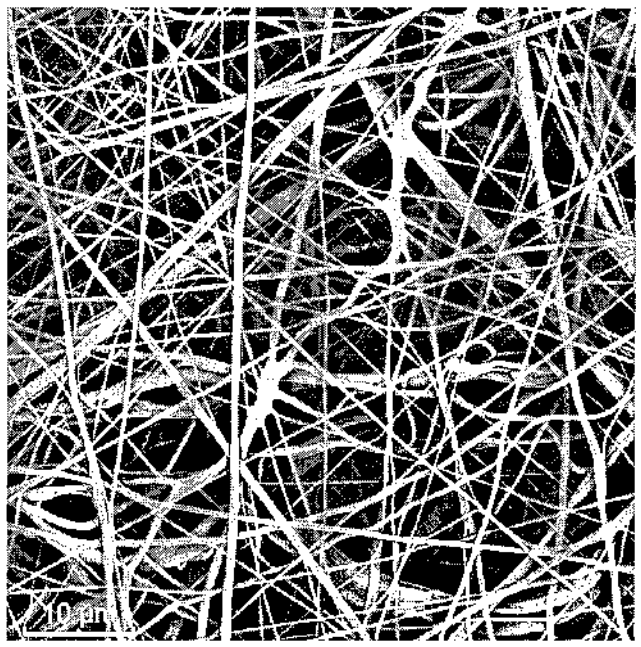

Fig. 2. SEM image of the PUR nanofiber mat produced by electrospinning process.

2.3. *Filter sample characterization*

Nanofiber based filter, prepared through the electrospinning process, has been characterized by the Scanning Electron Microscope (Vega II, Tescan, Czech republic), as visible in Fig. 2. The obtained SEM picture has consequently been used for the fiber diameter/pore size distribution determination using recently proposed digital image analysis technique (Sambaer et al., 2010). The obtained basic characteristics for the analyzed filter samples are summarized in Fig. 3(a) and (b); the produced filter sample has average fiber diameter size (293 nm), number average and biggest pore sizes (473 and 3478 nm, respectively), mass area (3.14 g/m²) and thickness (20 |um) determined from SEM side view sample image.

2.4. *Filtration efficiency*

Experimental particle penetration efficiency of fabrics was determined according to EN 779 standard at the constant air flow rate 5.7 cm/s. Aerosol particles were produced from di-ethyl-hexyl-seba- cate by a pneumatic aerosol generator. Size distribution of particles was measured before and after the fabric with the optical particle analysers—particle counters LAS X, manufactured by Particle Measuring Systems (USA), for small particles 0.1-0.4 pm and APS, manufactured by TSI (USA), for bigger particles 1.2-8.3 pm. The measurement results were reported as the collecting efficiency of fabric (%). The measured filtration efficiency curve is depicted in Fig. 3(c) (air flow rate 5.7 cm/s, pressure drop 316 Pa).

3. 3D structure model development from SEM pictures

The following strategy has been proposed for the realistic 3D model representation of produced PU based nanofiber electrospun mat

First, the original SEM sample image of the filter (see Fig. 2 as an example) is converted to a black and white image by applying a proper threshold level (equal to average grayscale value as suggested in (Ghasemi-Mobaralceh et al., 2007)) in order to emphasize only the top fibers from the others.

Second, using the converted black and white image, fiber centerlines pixels (which are always connected to each other) are determined by the algorithm developed by Ignacio et al. (2010) (see Fig. 4). The continuous centerline curves for each individual fiber (or its part) are determined by the grouping of those centerline pixels having only two neighbor pixels (i.e.

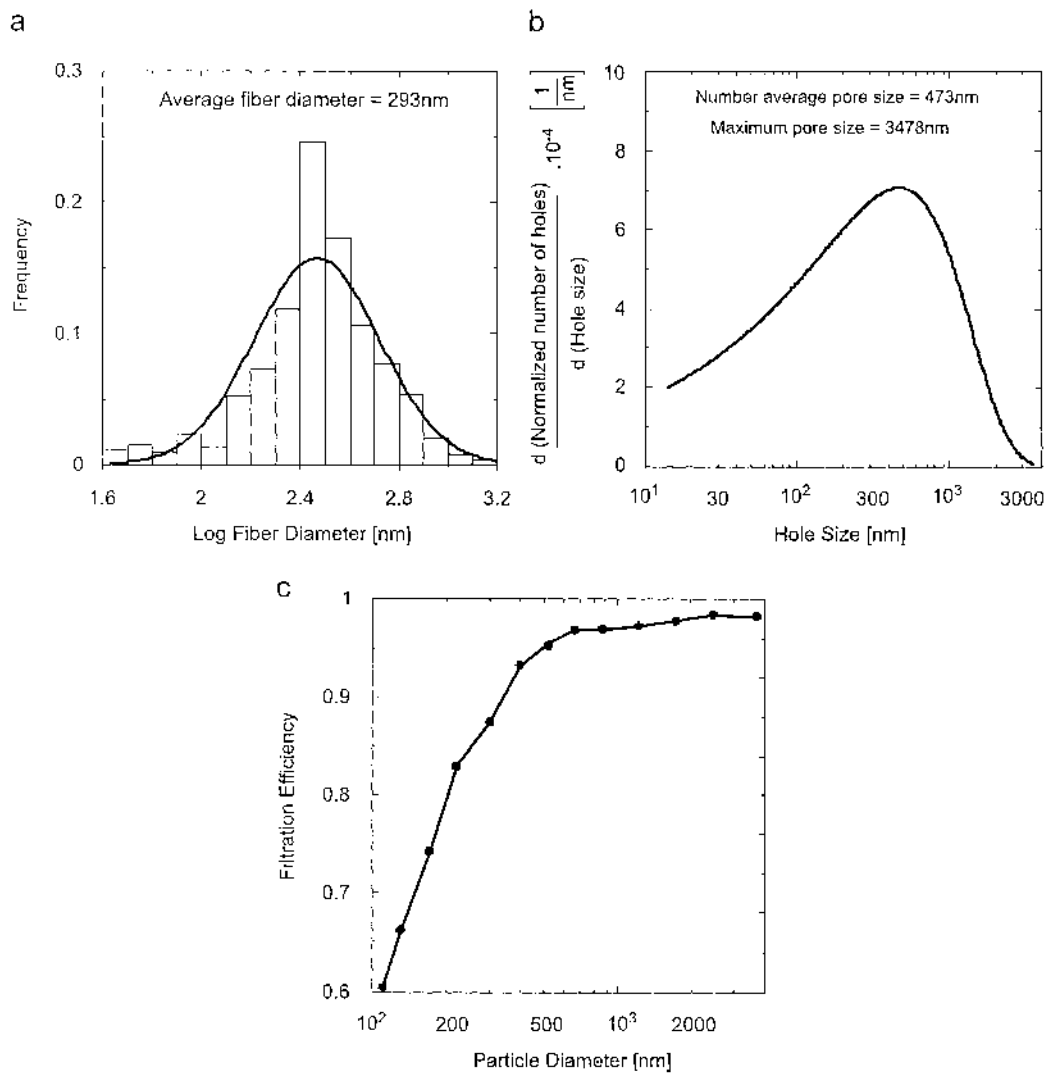

Fig. 3. Basic characteristics for PUR nanofiber mat: (a) Fiber diameter distribution; (b) pore size distribution and (c) filtration efficiency.

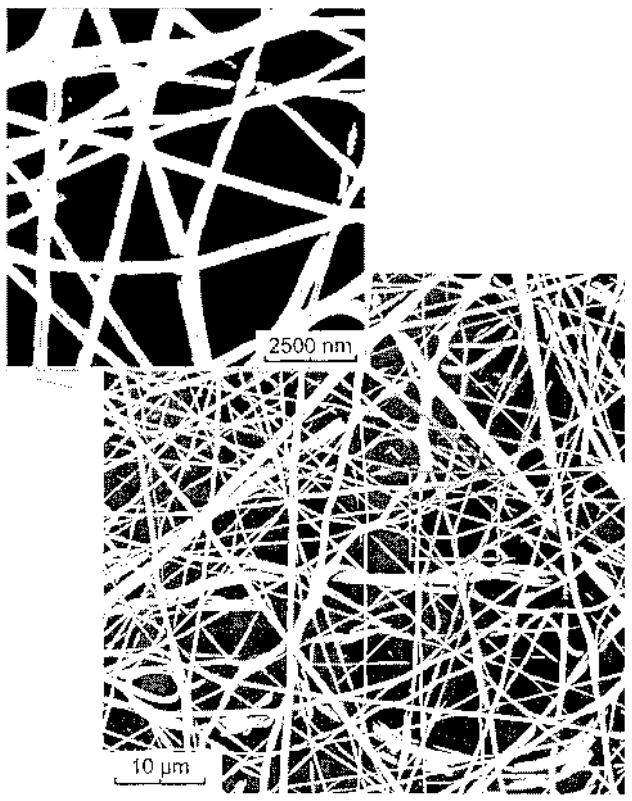

Fig. 4. Visualization of the converted black and white SEM image of the PUR nanofiber mat (depicted in Fig. 2) together with particular fiber centerlines.

branching is eliminated on the centerline curve). This reduces the complexity of the 3D structure model significantly because each fiber is represented by the limited number of sections. Moreover, it helps to recognize the sieve during the particle filtration modeling (because different fibers or their parts can be easily identified) and the distance calculation between different fibers/fiber parts (which is required for the force balance between the fiber and filtered particle) can be easily determined through direct availability of normal direction with respect to particular centerline curve (represented by the simple line for example in the most simplest case).

Third, 3D shape of each fiber section is created by the rotation of particular average diameter circle along every corresponding centerline pixel in the depth direction. The particular average diameter circle is determined from the number of different circles, which are localized in the particular centerline pixels and locally represents the fiber section diameters. In other words, all fiber sections are viewed in the proposed 3D structure model as mutually connected tubes having different diameters (see Fig. 5).

Full 3D nanofiber based nonwoven filter model is created by stacking limiting number of individual 3D nanofiber layers on each other with particular space between them in such a way that the mass area and final thickness of the 3D filter model is equal to the real sample (see Fig. 6). The proper and realistic representation of the fiber curvature, varying fiber diameter and specific shape of the cross section points are the main advantages of the proposed 3D structure model. Moreover, the 3D model is simply given by x,y,z centerline pixel coordinates (for one layer, all pixels lies on one plain) having information about the fiber diameter and particular

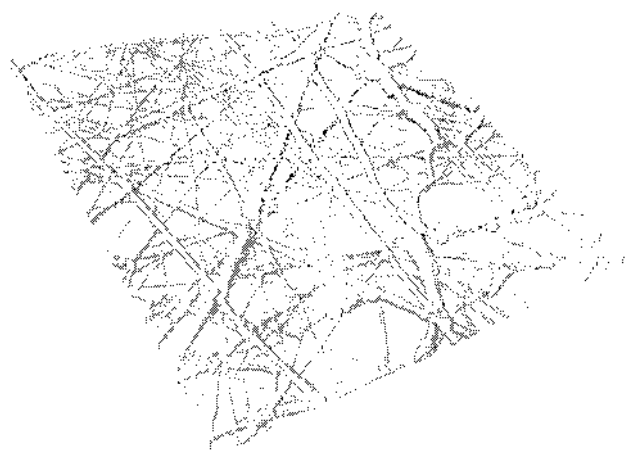

Fig. 5. Visualization of one **3D** nano fiber layer created from the converted black and white SEM image (depicted in Fig. 4).

fiber (or its part) to which they belong. This makes proposed model utilization in the particle filtration modeling very simple and effective.

It should also be mentioned that in order to build the 3D structure model from SEM picture successfully, the following requirements for the SEM image has to be fulfilled:

- The perpendicular rather than angled view should be preferred. This minimize the light reflection at the fiber edges, which can disturb the global threshold process during converting the grey scale SEM image to binary image leading to creation of artificial structures.
- Top fibers should be lighter (ideally having constant grayscale value) than bottom fibers and background. This allows precise extraction of top fibers only from SEM image for consequent creation of one 3D layer without creation of artificial structures. For this purpose, Back-Scattered Electron (BSE) detector for electron microscopy scanning can be utilized.

4. Flow field calculation

In general, four different flow regimes around the fibers exist depending on the fiber diameter and gas thermal and pressure conditions (Hosseini and Tafreshi, 2010a; Brown, 1993; Maze et al., 2007): continuum flow regime ($J_{(n}$<10~3), slip-flow regime (10~3 <K_n< 0.25), transition regime (0.25 < I<$_n$ <10) and free molecule regime (K_n > 10), where K_n is Knudsen number representing the ratio of the gas molecules mean free path and fiber diameter (see Eq. (6) for exact definition). Due to the fact that PU based nanofiber filters (prepared in this work by electrospinning process with average fiber diameter about 300 nm) operate at low pressure drops only, hydrodynamics conditions lies in the slip/transition/free molecular flow regime. Maze et al. (2007) concluded that for such flow condition, the influence of the fibers on the flow field is negligible because of significant slip occurrence at the fiber surface, thus uniform gas flow field can be considered in this work, as visible in Fig. 7.

In order to calculate particle position at each time step due to drag force exerted by the flow and the Brownian forces (assuming a constant air flow), all the time intervals At are divided into two parts by a single random coefficient (which is constant for each particle) LTe[0;1[in order to shift the Brownian motion sampling. The following solution taken from (Maze et al., 2007) has been utilized for these two time intervals:

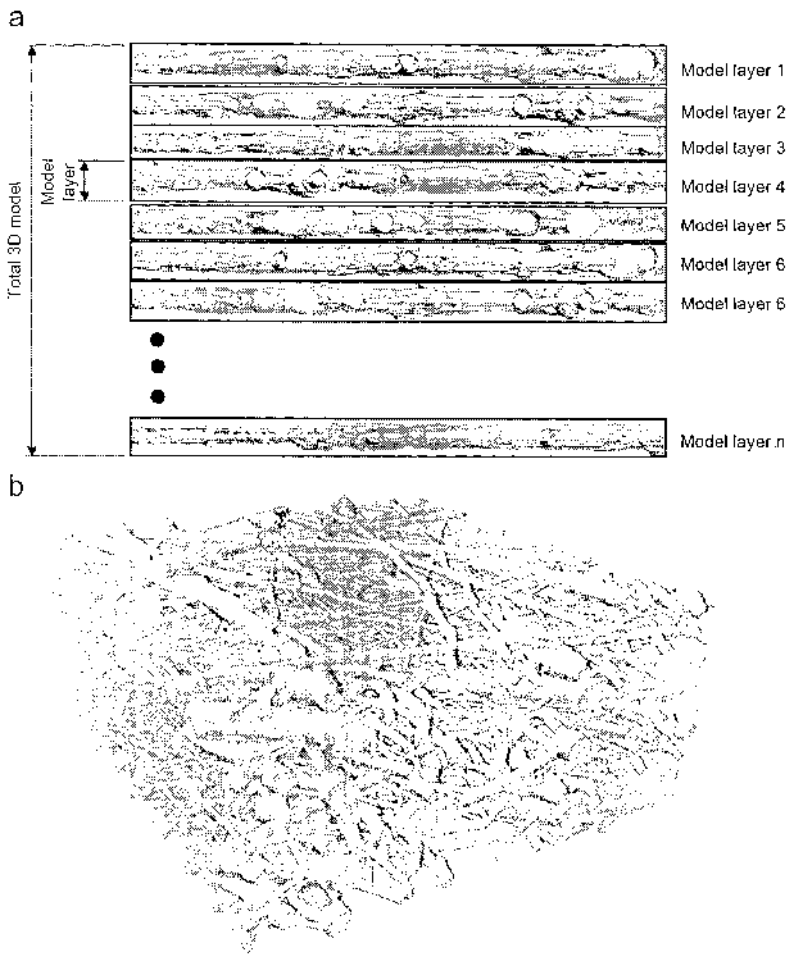

Fig. 6. Full 3D model for PUR nanofiber mat: (a) Side view and (b) perspective view (number of layers = 10).

Time interval $[j\Delta t;\ (j+U)\Delta t]$.

$$v_{i_p}((j+U)\Delta t) = \left(v_{i_p}(j\Delta t) - v_{i_f} - \frac{F_{b_i}}{\beta}\right)e^{(-\beta U\Delta t)} + \frac{F_{b_i}}{\beta} + v_{i_f}, \tag{1}$$

$$x_{i_p}((j+U)\Delta t) = \left(\frac{v_{i_p}(j\Delta t) - v_{i_f} - \frac{F_{b_i}}{\beta}}{\beta}\right)(e^{(-\beta U\Delta t)} - 1) - \left(\frac{F_{b_i}}{\beta} + v_{i_f}\right)U\Delta t + x_{i_p}(j\Delta t), \tag{2}$$

Time interval $[(j+U)\Delta t;\ (j+1)\Delta t]$.

$$v_{i_p}((j+1)\Delta t) = \left(v_{i_p}((j+U)\Delta t) - v_{i_f} - \frac{F_{b_{i+1}}}{\beta}\right)e^{(-\beta(1-U)\Delta t)} + \frac{F_{b_{i+1}}}{\beta} + v_{i_f}, \tag{3}$$

$$x_{i_p}((j+1)\Delta t) = \left(\frac{v_{i_p}((j+U)\Delta t) - v_{i_f} - \frac{F_{b_{i+1}}}{\beta}}{\beta}\right)(e^{(-\beta(1-U)\Delta t)} - 1) + \left(\frac{F_{b_{i+1}}}{\beta} + v_{i_f}\right)(1-U)\Delta t + x_{i_p}((j+U)\Delta t), \tag{4}$$

where v_{if} and v_{ip} are, respectively, the fluid and particle velocities in the x, y or z direction,

$$\beta = \frac{18\eta}{d_p^2\rho_p C_c} \tag{5}$$

is the relaxation frequency of the particle, d_p and p_p are the particle diameter and density, respectively, rj is liquid viscosity, $C_c = 1 + /C_n(1.275 + 0.4e^{(\sim 11/i<n)})$ is an empirical Cunningham slip correction factor, $I<_n$ is the fiber Knudsen number

$$K_n = \frac{2\lambda}{d_f} \tag{6}$$

where d_f is fiber diameter and X is the mean free path of gas molecules

$$\lambda = \frac{RT}{\sqrt{2}N_a\pi d_m^2 p} \tag{7}$$

where R *is* the gas constant, T the temperature, N_a the number of Avogadro, p the pressure and d_m the collision diameter of an air molecule ($3.7.10^{\sim 10}$ m).

F&$_{i+1}$ is the Brownian white noise excitation due to the impact of air molecules on the particle defined according to Li and Ahmadi (1992), Ounis and Ahmadi (1990), Ounis et al. (1991) as

$$F_{b_i} = \varsigma_i\sqrt{\frac{\pi S_{nn}}{\Delta t}}, \tag{8}$$

where q are zero-mean, unit-variance independent Gaussian random numbers, S_{nn} is the spectral intensity (characterizing the noise intensity) defined as

$$S_{nn} = \frac{3kT\beta}{\pi d_p^3\rho_p}. \tag{9}$$

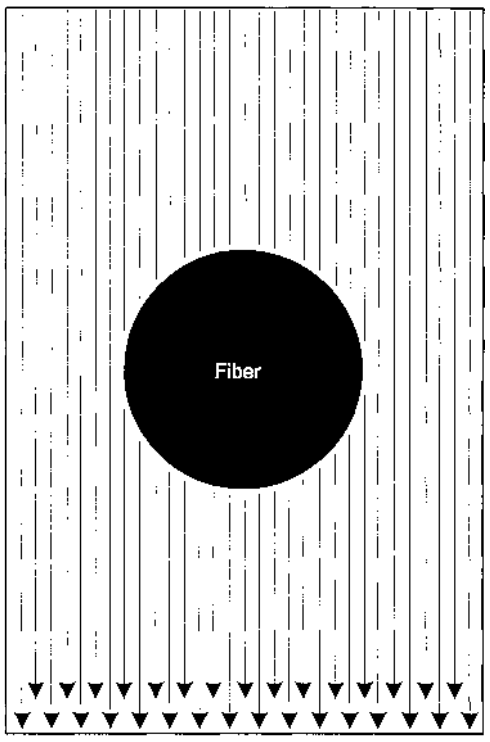

Fig. 7. Assumed air flow field around the fiber.

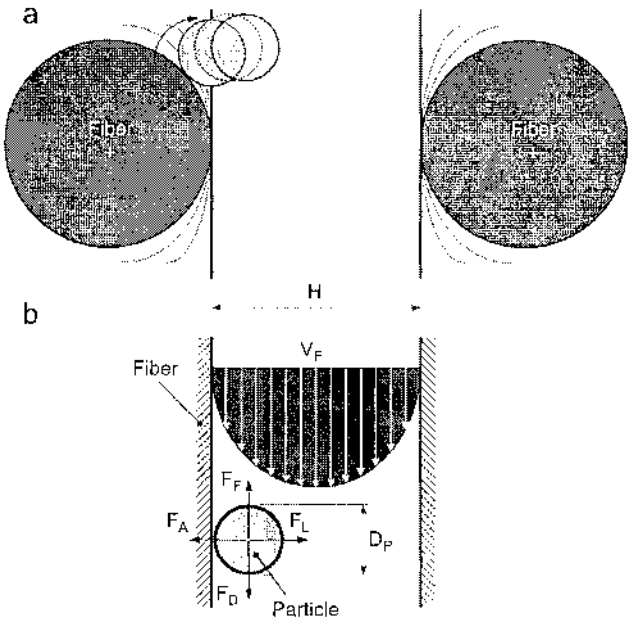

Fig. 8. Visualization of the particle movement along the fiber, (a) Tube pore definition *(H*—tube diameter, *L*—tube length); (b) particle-fiber force balance visualization inside the tube pore.

where *k* is the Boltzmann constant and *T* the temperature. It should be mentioned that the particles are not allowed to escape the simulation box through the sides; if this happened, their velocity vector is mirrored to move them back inside, as suggested in Maze et al. (2007).

5. Particle-fiber interaction modeling

The force balance, suggested by Altmann and Ripperger (1997) is accommodated here (see Fig. 8) for capturing particle-fiber interactions. It is considered here that the flow through the particular pore can be viewed as the Poiseuille flow in a 2D duct, which is characterized by the gap distance, *H*, and its length L In order to calculate reduced gas viscosity, 77, (due to the slip) correctly at high Knudsen numbers (K_n>0.01), the following viscosity definition equation proposed by McNenly et al. (2005) has been utilized for Poiseuille flows:

$$\eta = \eta'[a_0 + a_1 \arctan(a_2 K_n^{a_3})] \tag{10}$$

where *if* is the gas viscosity at given pressure and temperature, a_0= 1.066, =0.679, a_2= -2.082, a_3== 0.866.

In the force balance model, four different forces are considered; the drag force, F_D, the lift force, F_L, the adhesion (van der Waals) force, F_a, and the friction force F_f, which are defined in the following way.

5.1. Drag force, F_D

Drag force, F_D, starts to act on the fiber intercepted particle due to pressure driven shear flow occurring inside the pore having average diameter *H* because velocity between the solid particle and the fluid starts to be different. According to theoretical and experimental work of Rubin (1977), Altmann and Ripperger

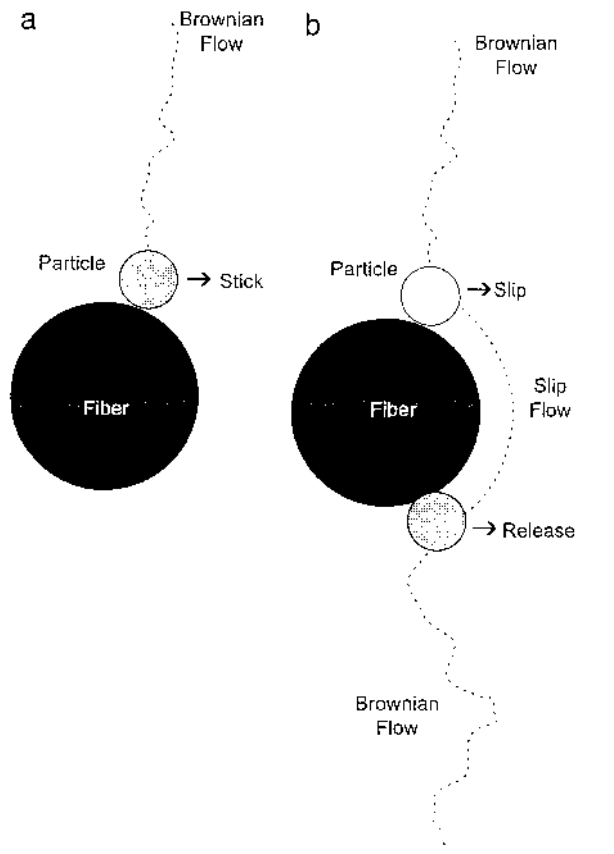

Fig. 9. Visualization of two possible particle-fiber configurations; (a) Particle sticks at the fiber and (b) particle slips along the fiber.

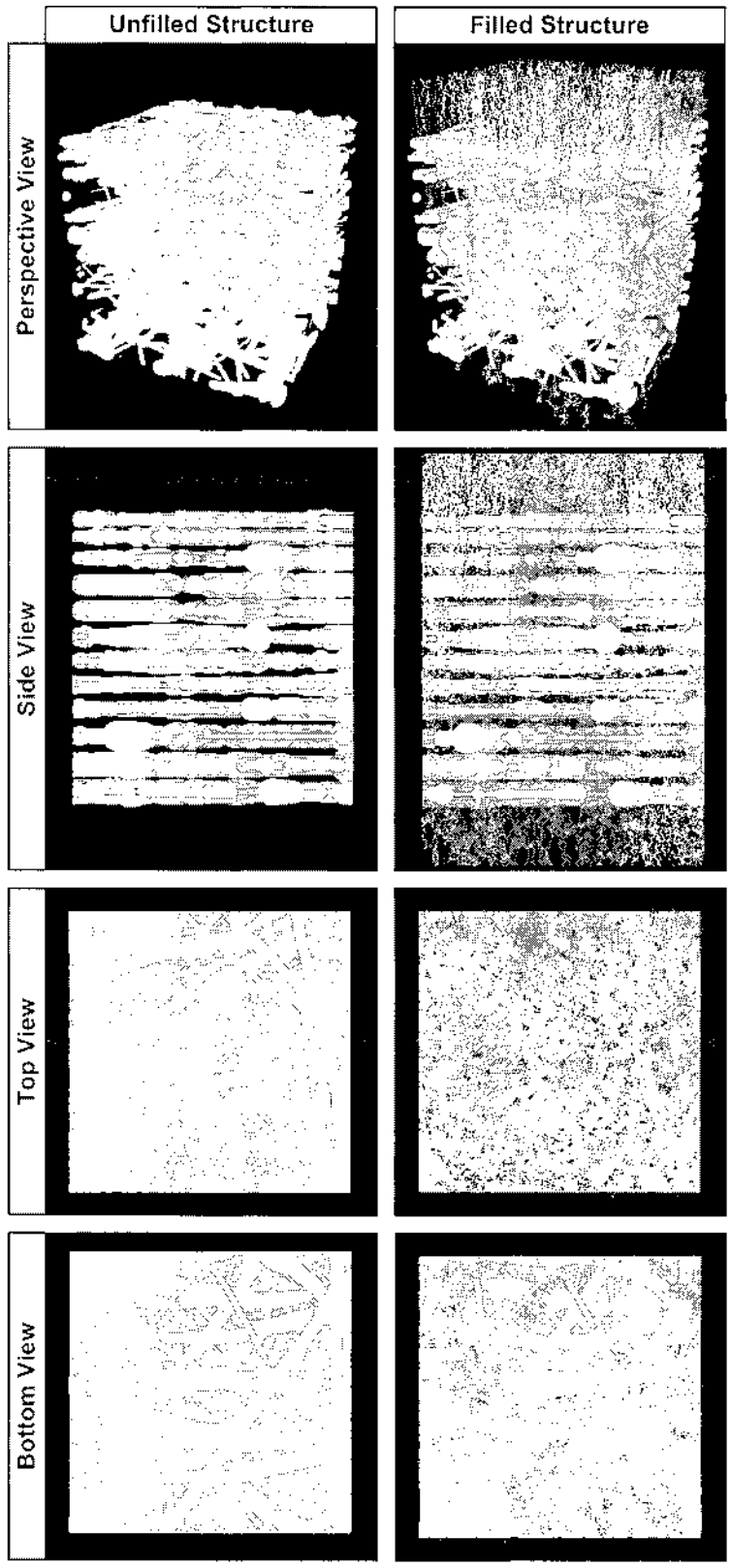

Fig. 10. Flow path lines through the medium colored by particle sizes (50 nm—**blue**, 200 nm—green, 500 nm—red). (For interpretation of the references to color in this figure legend, the reader is referred to the web version of this article.)

(1997), the drag force can be expressed in the following way:

$$F_D = 3.16\pi\tau_w d_p^2$$

where τ_W is local fiber wall shear stress, which can be calculated from the Newtonian law as

$$\tau_w = \mu\dot{\gamma}_i \quad (12)$$

where γ represents shear rate at the fiber wall. Note that the characteristic pore size dimension H is determined here as the perpendicular distance between the interception particle-fiber point and surrounding fiber, which represents the second part of the pore. It also should be mentioned that the assumption about the constant flow velocity field has been relaxed for the force balance calculation in order to mimic different levels of slip and drag force intensity according to actual fiber diameter (Knudsen number) dependent air viscosity.

5.2. *Lift force, F_L*

According to the theoretical and experimental analysis of Rubin (1977), Altmann and Ripperger (1997 and McLaughlin, 1993), the lift force is caused by the shear flow and can be calculated as follows

$$F_L = \frac{0.761\tau_w^{1.5} d_p^3 \rho_f^{0.5}}{\eta} \quad (13)$$

where ρ_f is density of the fluid.

5.3. *Adhesive force F_A*

The estimation of the this force is complicated because different parameters such as particle-fiber shape, particle-fiber roughness, adhesion distance, number of contact points, etc. may influence the adhesive force strongly (Altmann and Ripperger, 1997). Neglecting the electrostatic interactions, the adhesive forces can be evaluated by calculating van der Waals force between two ideal spheres as follows

$$F_A = \frac{\hbar\overline{\omega} d_p}{32\pi a^2} \quad (14)$$

where $M1$ is the Lifschitz-van der Waals constant (10^{-2} J) and a is the adhesive distance (0.4 nm (Altmann and Ripperger, 1997; Brown, 1993)).

5.4. *Friction force F_F*

The friction force is caused by the action of the forces acting towards the fiber surface (van der Waals force F_A in this case).

$$F_F = \mu F_A \quad (15)$$

where ji is the friction coefficient ($0 < \mu_A < 1$).

The particle is considered to be intercepted by the fiber when the lift force is lower/equal than the adhesion force, $F_L < F_A$, or the drag force is lower/equal than the friction force, $F_D < F_F$ (see

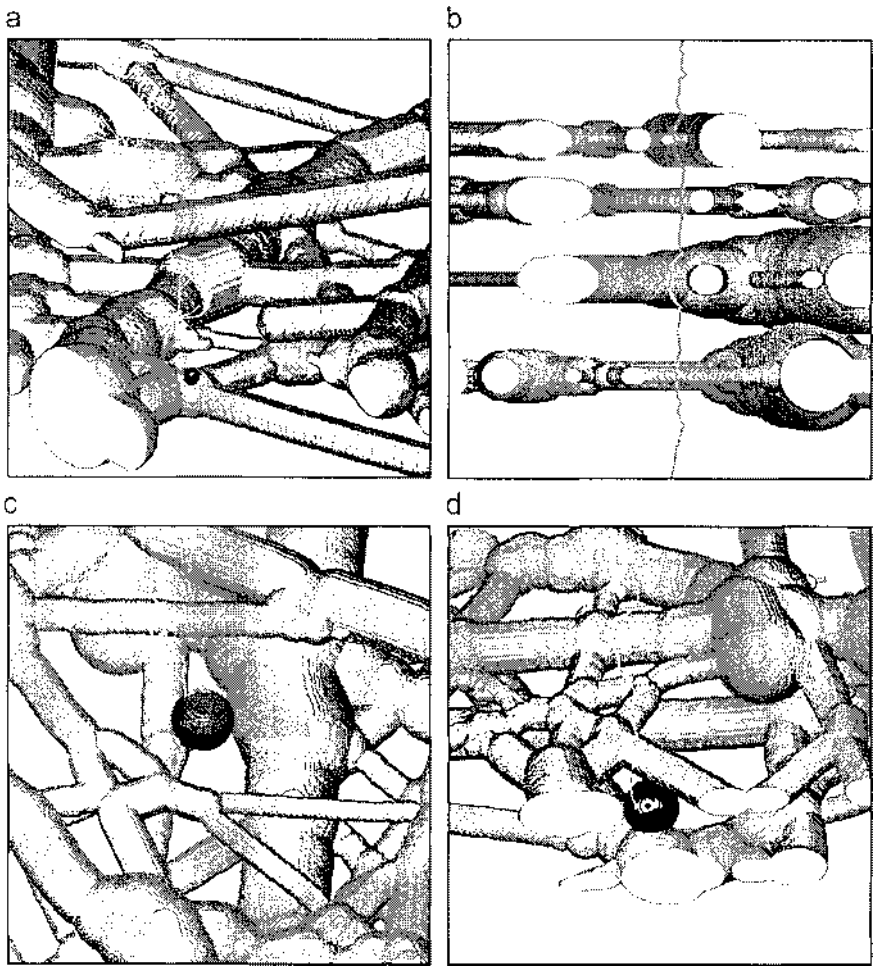

Fig. 11. Detail view of the flow path lines: (a) Captured 100 nm particle at the fiber; (b) 500 nm particle path line, which has passed the filter due to slip around the fiber; (c) sieve of the 500 nm particle at one model layer and (d) sieve of the 500 nm particle between 2 different model layers.

Fig. 9(a)). On the other hand, if the lift force is higher than the adhesion force *(F_L > F_A)* or the drag force is higher than the friction force (F_d > F_f), the particle starts to slip around the fiber in the perpendicular plane with respect to that fiber and the particle is always released from the fiber in the horizontally mirrored position with respect to initial sticking point between the particle and fiber as visible in Fig. 9(b). This is due to the applied assumption that the slipping particle follows the air path line, which is always released from the fiber in the horizontally mirrored position with respect to initial sticking point as depicted in Fig. 7. It also should be mentioned that particle catching due to sieving is considered when at least two connection points between fiber 1 - particle-fiber2 are identified during the particle motion modeling.

6. Comparison between experimental and theoretical data, parametric study and conclusions

In this part, the suggested particle filtration modeling approach will be tested. In the first step, the 3D structure model for manufactured PU filter samples according to methodology described above has been generated. Efficiency of the filter is theoretically determined by the number of particles, which can be captured inside the filter (Maze et al., 2007)

$$E = \frac{N_{in} - N_{out}}{N_{in}} \qquad (16)$$

where N_{in} and N_{out} are the number of entering and exiting particles, respectively. 100 different groups of particles having diameter linearly varying from 20 to 1000 nm in logarithmic scale (1000 identical sphere particles per one group) were injected at the filter inlet (28 x 28 jum²). The following reference filtration parameters (which correspond to the filtration experiment described above) have been utilized: v_{if} =0.057 m/s, p −101,325 Pa, 7=300 K, /i=0.0025, p_p = 1000 kg/m³, ^=3.8 10"⁵ Pa s. Each particle has been traced through the clean filter, i.e. particle-particle interactions have been neglected, and number of exiting particles was determined in order to calculate filter capture efficiency as a function of particle size. Fig. 10 is an example of the simulation results, where a number of particle path lines having different sizes (50, 200 and 500 nm) are visualized. Detail view of the possible individual particle path lines is provided in the Fig. 11.

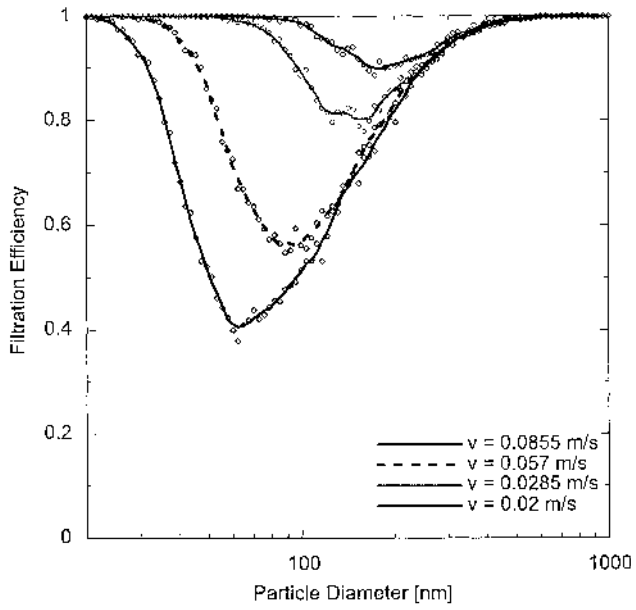

Fig. 13. Predicted effect of the air velocity on the PUR electrospinning sample filtration efficiency (mass area=3.14 g/m², sample thickness = 20 [im, p=101,325 Pa, T=300 K, *fi*=0.0025, p_p=1000 kg/m³, ^'=3.8 10"⁵ Pa s). Lines represent curve fit for particular calculated data points (running average fit with window width equal to 5).

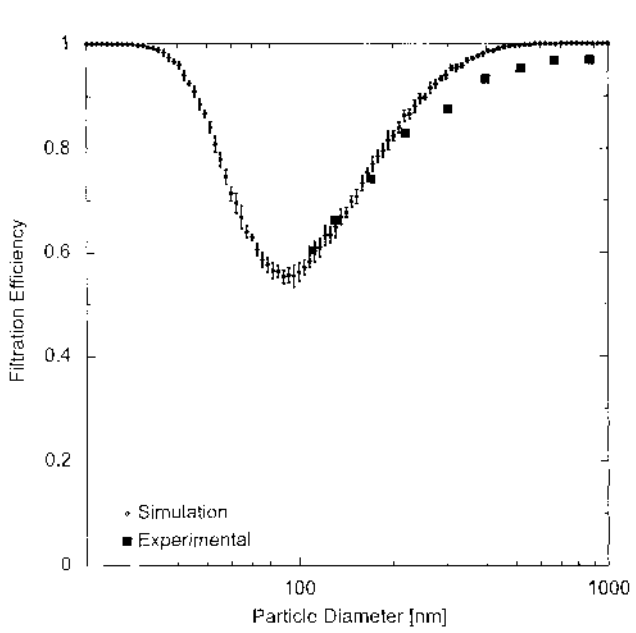

Fig. 12. Comparison between measured and predicted filtration efficiency curves for the PUR electrospinning nonwoven sample (mass area = 3.14 g/m², sample thickness = 20 jj.m, v_{if} =0.057 m/s, p = 101,325 Pa, 7=300 K, ¿¿=0.0025, p_p = 1000 kg/m³, /7' =3.8 10~⁵ Pa s).

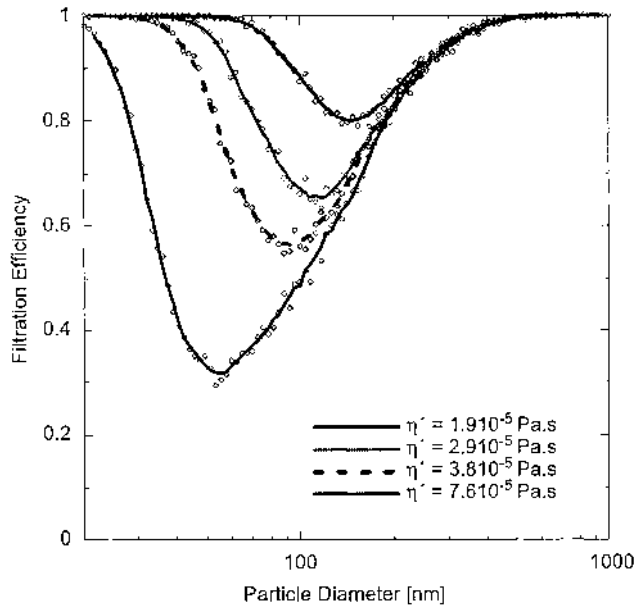

Fig. 14. Predicted effect of the air viscosity on the PUR electrospinning sample filtration efficiency (mass area=3.14 g/m², sample thickness=20 jam,v_{if} =0.057 m/s, p = 101,325 Pa, 7=300 K, ¿¿=0.0025, p_p = 1000 kg/m³). Lines represent curve fit for particular calculated data points (running average fit with window width equal to 5).

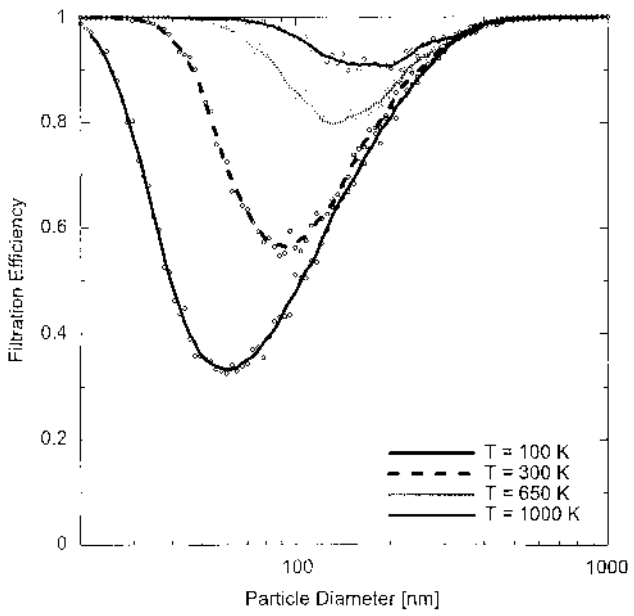

Fig. 15. Predicted effect of the air temperature on the PUR electrospinning sample filtration efficiency (mass area = 3.14 g/m², sample thickness = 20 jim, v_{if} =0.057 m/s, *p* —101,325 Pa, *f.i* — *0.00*25, p_p = 1000 kg/m³, *tj'= 3.8* 10~⁵ Pa s). Lines represent curve fit for particular calculated data points (running average fit with window width equal to 5).

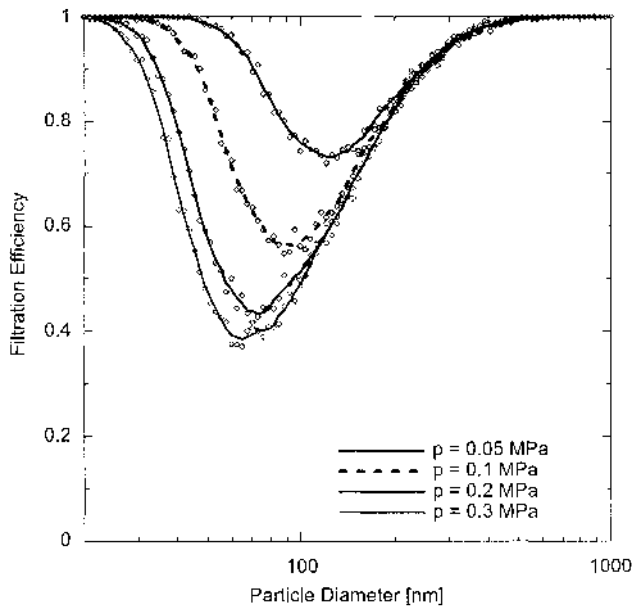

Fig. 16. Predicted effect of the air pressure on the PUR electrospinning sample filtration efficiency (mass area=3.14 g/m², sample thickness=20 p,m, $v_{/f}$ =0.057 m/s, 7=300 K, ¿¿=0.0025, p_p = 1000 kg/m³, *rj'=3.*8 10⁻⁵ Pa s). Lines represent curve fit for particular calculated data points (running average fit with window width equal to 5).

Comparison between experimentally and theoretically determined filter efficiency data for the tested sample is provided in Fig. 12. Note that simulations were repeated 10 times in order to obtain average values and standard deviations. It is nicely visible, that the model predictions are in very good agreement with the experimental data in the range of small particle sizes at which the Brownian force, rather than air flow field, dominantly influences the nanoparticles trajectory i.e. within the particle size range for which the assumption about a uniform air flow field is justifiable. Disagreement between predicted and measured filter efficiency for the large diameter particles can be explained by the error in the particle trajectory calculation, because the Brownian force vanishes in this case and air flow field starts to play the dominant role, or by the possible presence of big pores (defects) in the tested sample, which have not been SEM detected and thus not considered in the performed calculation.

In the second step, the effect of air velocity, viscosity, temperature, pressure and friction coefficient between the particle and fiber have been investigated theoretically by the proposed technique. For that purpose, the 3D structure model for the produced PU filter has been utilized. The theoretical predictions of the filtration efficiency are provided in Figs. 13-17. It can be clearly seen that increase in air velocity, viscosity and air pressure leads to filtration efficiency decrease, because of increased drag/lift forces and reduced Brownian motion intensity, whereas the increase in the air temperature and particle-fiber friction coefficient leads to filtration efficiency enhancement due to increased Brownian motion intensity and reduced particle slip, respectively, and vice versa. Clearly, the air velocity, viscosity and particle-fiber friction coefficient seems to have the highest impact on the filtration efficiency of the tested filter. In more detail, the obtained theoretical results with respect to friction coefficient effect on the filtration efficiency depicted in Fig. 17 suggests that particle- fiber surface modification can significantly influence filtration efficiency especially for particles having small size (< about 200 nm in this specific case).

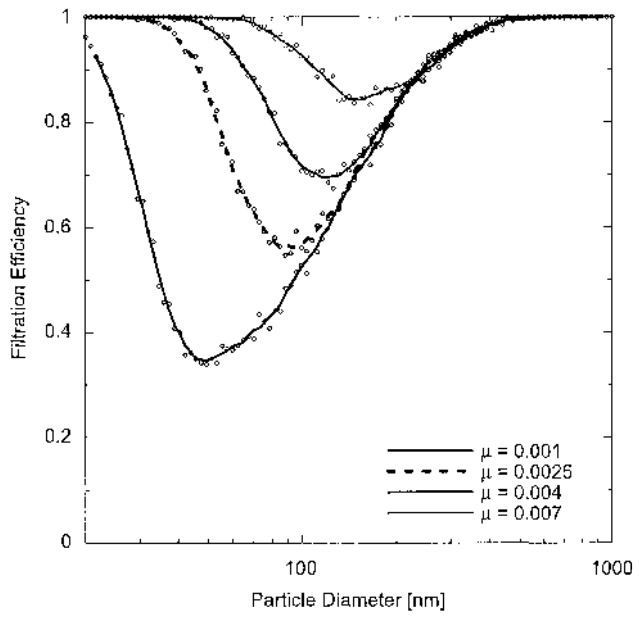

Fig. 17. Predicted effect of the friction coefficient on the PUR electrospinning sample filtration efficiency (mass area=3.14 g/m², sample thickness=20 ^im, $v_{,-f}$ =0.057 m/s, p = 101,325 Pa, 7=300 K, p_p=1000 kg/m³, Ty = 3.8 10"⁵ Pa s). Lines represent curve fit for particular calculated data points (running average fit with window width equal to 5).

It should also be mentioned that the predicted trends for air temperature/velocity with respect to filtration efficiency are in good quantitative agreement with previous studies (Maze et al., 2007; Thomas and Yoder, 1956; Sinclair, 1970).

7. Conclusions

In this work, a nanofiber nonwoven based PU filter has been produced using electrospinning process. A new methodology to create simple 3D structure model from SEM image of the filter has been proposed. Full 3D particle filtration modeling using such a 3D structure model representing real filter structure has been utilized considering slip/transition/free molecular flow regime, particle- fiber interactions, air/particle slip at the fiber surface, sieve and homogenous flow field. The obtained theoretical predictions for the filtration efficiency have been compared with the corresponding experimental data and good agreement between both data sets have been obtained, especially at the particle size range for which the applied model assumptions are valid. The effect of different factors such as air velocity, viscosity, temperature, pressure and particle-fiber friction coefficient has been theoretically investigated for the produced PU nanofiber based filter. It has been revealed that the change of the particle-fiber friction coefficient (which can be done by particle-surface modification for example) has one of the highest effects on the filtration efficiency (within the range of all tested parameters and their values), especially for nanoparticles having diameter less than about 200 nm for the studied conditions and filter structure. It is believed that the proposed modeling tools in this work will help to evaluate filtration efficiency of different nanofiber nonwoven based structures from their SEM images in order to provide useful guidelines for their optimization and enhancement.

Acknowledgments

The authors wish to acknowledge Grant Agency of the Czech Republic, Grant no. P108/10/1325 and the Ministry of Education CR, Grant no. MSM 7088352101, for the financial support, as well as to Matti Lehtimaki and Hannu Salmela from VTT Technical Research Centre of Finland, Tampere, for their work on the experimental filtration efficiency measurements. We would also like to acknowledge the university college KHBO, Belgium for their support

References

Andrady, A.L., 2008. Science and Technology of Polymers Nanofibers. John Wiley & Sons, Inc., New Jersey.

Ashari, A., Tafreshi, H.V., 2009. A two-scale modeling of motion-induced fluid release from thin fibrous porous media. Chemical Engineering and Science 64,2067-2075.

Altmann, J., Ripperger, S., 1997. Particle deposition and layer formation at the crossflow microfiltration. Journal of Membrane Science 124, 119-128.

Brown, R.C., 1993. Air Filtration: An integrated Approach to the Theory and Applications of Fibrous Filters. Pergamon Press, Oxford.

Fotovati, S., Tafreshi, H.V., Pourdeyhimi, B., 2010. Influence of fiber orientation distribution on performance of aerosol filtration media. Chemical Engineering and Science 65, 5285-5293.

Ghasemi-Mobarakeh, L., Semnani, D., Morshed, M., 2007. A novel method for porosity measurement of various surface layers of nanofibers mat using image analysis for tissue engineering applications. Journal of Applied Polymer Science 106, 2536-2542.

Hosseini, S.A., Tafreshi, H.V., 2010a. Modeling permeability of 3-D nanofiber media in slip flow regime. Chemical Engineering and Science 65, 2249-2254.

Hosseini, S.A., Tafreshi, H.V., 2010b. 3-D simulation of particle filtration in electrospun nanofibrous filters. Powder Technology 201, 153-160.

Ignacio, Arganda-Carreras, Rodrigo, Fernandez-Gonzalez, Arrate, Munoz-Barrutia, Carlos, Ortiz-De-Solorzano, 2010. 3D reconstruction of histological sections: application to mammary gland tissue. Microscopy Research and Technique 73, 1019-1029.

Jaganathan, S., Tafreshi, H.V., 2008. Modeling liquid porosimetry in modeled and imaged 3-D fibrous microstructures. Journal of Colloid and Interface Science 326, 166-175.

Jaganathan, S., Tafreshi, H.V., Pourdeyhimi, B,, 2008. A realistic approach for modeling permeability of fibrous media: 3-D imaging coupled with CFD simulation. Chemical Engineering and Science 63, 244-252.

Li, A., Ahmadi, G., 1992. Dispersion and deposition of spherical-particles from the point sources in a turbulent chemical flow. Aerosol Science and Technology 16, 209-226.

Maze, B., Tafreshi, H.V., Wang, Q., Pourdeyhimi, B, 2007. A simulation of unsteady-state filtration via nanofiber media at reduced operating pressures. Journal of Aerosol Science 38, 550-571.

McNenly, M.J., Gallis, M.A., Boyd, I.D., 2005. Empirical slip and viscosity model performance for microscale gas flow. International Journal for Numerical Methods in Fluids 49, 1169-1191.

McLaughlin, J.B., 1993. The lift on a small sphere inwall bounded linear shear flows. Journal of Fluid Mechanics 246, 249-265.

Ounis, H., Ahmadi, G., 1990. A comparison of Brownian and turbulent-diffusion. Aerosol Science and Technology 13, 47-53.

Ounis, H., Ahmadi, G., Mclaughlin, J.B., 1991. Dispersion and deposition of Brownian particles from the point sources in a simulated turbulent channel flow. Journal of Colloid and Interface Science 147, 233-250.

Pich, J., 1966. Pressure drop of fibrous filters at small Knudsen numbers. Annals of Occupational Hygiene 9, 23-27.

Rubin, G., 1977. Widerstands und Auftreibsbeiwerte von Ruhenden Kugelformigen Partikeln in Stationaren, Wandnahen Laminaren Grenzschichten, Dissertation. TH Karlsruhe.

Sambaer, W., Zatloukal, M., Kimmer, D., 2010. The use of novel digital image analysis technique and rheological tools to characterize nanofiber nonwovens. Polymer Testing 29, 82-94.

Sinclair, D., 1970. Penetration of HEPA filters by submicron aerosols. Journal of Aerosol Science 1, 53-67.

Tafreshi, H.V., Rahman, M.S.A., Jaganathan, S., Wang, Q.., Pourdeyhimi, B., 2009. Analytical expressions for predicting permeability of bimodal fibrous porous media. Chemical Engineering and Science 64, 1154-1159.

Thomas, J.W., Yoder, R.E., 1956. Aerosolsize for maximum penetration through fiberglass and sand filters. American Medical Association Archives of Industrial Health 13, 545-549.

Wang, Cl, Maze, B., Tafreshi, H.V., Pourdeyhimi, B., 2007. On the pressure drop modeling of monofilament-woven fabrics. Chemical Engineering and Science 62, 4817-4821.

Wang, Q., Maze, B,, Tafreshi, H.V., Pourdeyhimi, B., 2006a. A note on permeability simulation of multifilament woven fabrics. Chemical Engineering and Science 61, 8085-8088.

Wang, Q., Maze, B., Tafreshi, H.V., Pourdeyhimi, B., 2006b. A case study of simulating submicron aerosol filtration via lightweight spun-bonded filter media. Chemical Engineering and Science 61, 4871-4883.

Zobel, S., Maze, B., Tafreshi, H.V., Wang, Q.., Pourdeyhimi, B., 2007. Simulating permeability of 3-D calendered fibrous structures. Chemical Engineering and Science 62, 6285-6296.